Structural health monitoring of glulam structures: analysis of durability and damage mechanisms

Guilhem Greffier, Luis Espinosa, Marianne Perrin, Florent Eyma

European Journal of Wood and Wood Products (2024) 82:2047–2063
https://doi.org/10.1007/s00107-024-02140-9

ORIGINAL ARTICLE

Structural health monitoring of glulam structures: analysis of durability and damage mechanisms

Guilhem Greffier[1] · Luis Espinosa[1] · Marianne Perrin[1] · Florent Eyma[1]

Received: 16 April 2024 / Accepted: 19 August 2024 / Published online: 5 October 2024

Abstract

In today's environmental context, the use of glulam or Glued Laminated Timber (GLT) as an alternative to conventional building materials could reduce the carbon footprint of engineering structures. However, this material is sensitive to outdoor exposure with moisture content variations inducing internal stresses and cracks and high moisture content increasing the risks of decay. This study therefore focuses on the development of a protocol to evaluate the effect of climatic conditions on the mechanical performance of the material. For this purpose, GLT samples were equipped with embedded sensors. Moisture and deformation sensors can accurately track wet-dry (W/D) cycles and their effects on deformation at adhesive joints. Samples are stored outdoors and mechanical tests are carried out after 6 months of aging. The results show an average reduction in flexural strength of about 10% compared to unaged specimens. Shear tests on the adhesive joints show a decrease in strength of more than 20%. The study of the fracture mechanisms also indicates a link between the type of fracture and the aging conditions of the specimens. These tests also validated a monitoring protocol that will allow, in the long term, to evaluate the impact of these cycles on the mechanical performance of GLT.

1 Introduction

Today, the use of wood, and particularly glulam, as an alternative to so-called "traditional" building materials such as concrete and steel, allows to reduce the environmental impact of engineering structures (Hurmekoski 2017; Hill 2019). Glulam is made up of finger-jointed and glued wooden slats, allowing to create spans and sections suitable for most short bridges (less than 50 m) (Gustafsson et al. 2010; Koch et al. 2016; Legg and Tingley 2020). There are studies on the long-term behavior of solid wood based on the Madison curve model (Wood 1947) for use classes 1 or 2 within the meaning of the EN 335 standard (EN 335 2013) which have made it possible to define the requirements of the calculation codes. However, the long-term behavior of glulam, particularly outdoors, is not sufficiently documented (Ehrhart et al. 2021). The safety factors applied to glulam in Eurocode 5 are derived from studies on solid wood (Racher et al. 1996; EN 1995-1-1 2005; EN 1995-2 2005). The specificities related to the composition of this material are therefore not considered. In addition to the common problems of wood with regard to humidity such as fungal and insect attacks, glulam, by its constitution, is particularly sensitive to wetting/drying (W/D) cycles. Indeed, the cycle-related shrinkage-swelling mechanisms generate stresses at the interfaces between the lamellae. This leads to delamination and cracking that damages the sections and degrades their mechanical properties (SETRA 2006; Angst-Nicollier 2012; Kánnár et al. 2019; Fortino et al. 2020).

If preventive measures such as weather protections for wooden structures should be one of the main considerations for the design of glulam structures, glulam instrumentation remains essential to ensure a structural health monitoring (SHM) of unprotected glulam, to assess the efficiency of preventive measures and to anticipate maintenance operations. In this context, for several years now, glulam structures have been monitored with moisture sensors using screw type electrodes (Tannert et al. 2011; Fragiacomo et al. 2011; Franke et al. 2013; Bjorngrim et al. 2016). These studies highlight W/D cycles related to climatic conditions. However, these sensors mainly measure surface moisture and require drilling to be able to make depth measurements that never exceed 20 cm as they can affect structural

✉ Guilhem Greffier
guilhem.greffier@iut-tarbes.fr

[1] Institut Clément Ader (ICA); Université de Toulouse; CNRS, UPS, INSA, ISAE-SUPAERO, IMT Mines Albi , 3 rue Caroline Aigle, Toulouse 31400, France

integrity. Glulam specific instrumentation has therefore been developed at the Clément Ader Institute (Li et al. 2017; Uwizeyimana et al. 2020). The system measures the moisture in a beam via patch-type resistive sensors embedded in the thickness of the glue joint. The advantage of this system is that it allows the mapping of moisture in structural elements with sensors that can be installed in large numbers without any effect on the material integrity (Uwizeyimana et al. 2020). The integration of strain gauges into the thickness of the adhesive joint also allows to study of shrinkage-swelling phenomena that stress the joint (Uwizeyimana et al. 2023) The use of moisture sensors and gauges during accelerated W/D cycles highlights the potential of these sensors to provide monitoring in glulam timber. These tests showed the reliability of this instrumentation to follow accelerated W/D cycles and the considerable weakening of the mechanical bending properties related to these cycles. An average decrease in strength of 43.5% after 17 cycles, led to the realization of tests in real conditions. This instrumentation was therefore used in the framework of this work on medium-term tests under external climatic conditions on glulam samples. Monitored specimens, loaded and unloaded, are exhibited outdoors on the site of the IUT of Tarbes. The exposure conditions of the specimens are evaluated using meteorological data collected at the Tarbes-Ossun-Lourdes site. The objective of this work is therefore to identify the impact of natural W/D cycles combined with the effects of loading on the evolution of the mechanical properties of glulam. In this context a 5 year long ageing experiment is being carried out in a "worst-case scenario" with unprotected glulam. This paper highlights the effects on shear strength of glue joints and static bending strength of glulam of the first 6 months of outdoor exposure.

The proper functioning and reliability of the outdoor instrumentation were evaluated during these 6 months of study. The data collected can be used to accurately track the effect of weather conditions on the humidity and deformation of the specimens. These results are compared with macroscopic observations on specimens. The evolution of the adhesive joint strength is measured in shear as well as the evolution of the 4-point bending strength.

2 Materials and methods

2.1 Glulam specimens

To evaluate the effect of outside exposure on the evolution of glulam mechanical performance, 198 specimens made of three Douglas fir lamellae bonded with polyurethane adhesive (KLEIBERT PUR 510 FiberBond) were manufactured. The number of specimens chosen allows us to carry out fracture tests every 6 months on 6 specimens for 5 years. This study therefore involves 24 samples tested after the first 6 months of ageing. The dimensions of the specimens are $30 \times 30 \times 480$ mm^3. These proportions have been determined in accordance with the EN 408 (2012) standard concerning flexural tests on glulam timber. The dimensions of the specimens and the manufacturing method are similar to those used by Uwizeyimana (2021) in accelerated durability testing. The lamellae are stabilized in a climatic chamber at 20 °C and 65% relative humidity (RH) before being glued. An amount of 200 g/m² of glue is distributed over the Douglas fir lamellae, then the specimens are pressed under a pressure of 10 bar for 8 h in accordance with the manufacturer recommendations for this glue and the methods used by glulam manufacturers. Douglas fir was chosen because it is naturally durable and suitable for outdoor use (Kutnik et al. 2011). Polyurethane glue is commonly used in the glulam industry (SETRA 2006). To assess the impact of W/D cycles and hygromechanical coupling (Armstrong and Christensen 1961; Grossman 1976; Pittet 1996) on the mechanical properties of glulam, the specimens are separated into three sets, exposed to different weathering conditions. The first set consists of 6 specimens, unprotected and outdoor exposed with a load of 60 daN in 4-point bending with a distance between lower and upper support of 135 mm (Fig. 1).

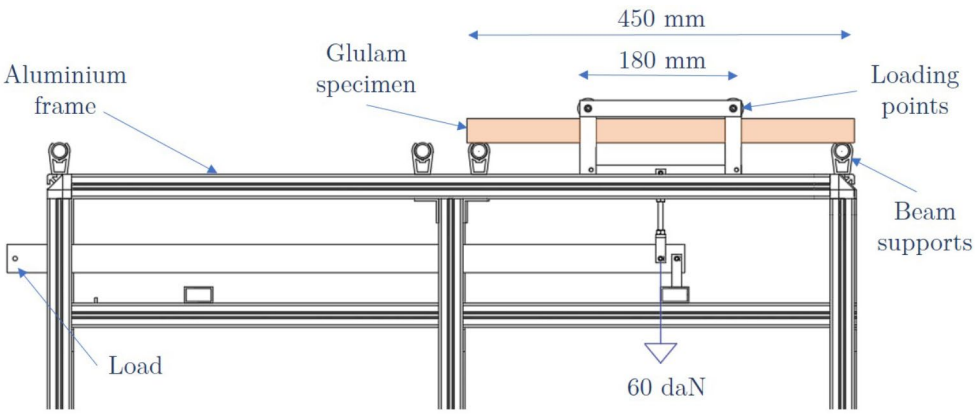

Fig. 1 Diagram of the outdoor loading system

This load was determined to avoid creep failure over the duration of the tests under severe exposure conditions (Hearmon and Paton 1964; Mårtensson 1994; Pittet 1996). The applied load is about 10% of the mean bending strength determined experimentally and is equal to 600 daN ± 80 daN. In order to approximate the conditions of use of bridges, the loading rate was also compared with the design standard at the Ultimate Limit States (ULS) of Eurocode 5.

The design flexural strength as defined by Eurocode 5 (EN 1995-1-1 2005) is defined as follows:

$$R_{fd} = \frac{R_{fk}.K_{mod}}{\gamma\, m} \quad (1)$$

Where:

- R_{fd} : The design flexural strength (MPa);
- R_{fk} : The characteristic flexural strength (MPa);
- $\gamma\, m$: The material safety factor;
- K_{mod} : The factor that considers the loading time and the class of service.

Considering the maximum strength class for Douglas fir (C24): $R_{fk} = 24MPa$, the material safety factor for GLT: $\gamma\, m = 1.25$ and the K_{mod} coefficient in service class 3 for long-term loading: $K_{mod} = 0.55$, the design flexural strength is $R_{f,d} = 10.56\ MPa$

The maximum bending stress must therefore be lower than the design strength to meet the reliability requirements of the Eurocode. In 4-point bending, this criterion is defined according to the following equation:

$$R_{f,d} \leq \frac{3\mathrm{F}a}{bh^2} \quad (2)$$

Where:

- $R_{f,d}$: The design flexural strength (in MPa);
- b and h: The width and height of the specimen (30 × 30 mm²);
- a: The distance between a lower support and the nearest upper support (135 mm);
- F: The applied force (N).

Considering the geometrical characteristics of the specimens and the loading device, the maximum applicable force within the meaning of Eurocode 5 is therefore 70.4 daN. The applied load of 60 daN corresponds to a loading rate of about 85% on these specimens. This load is therefore consistent with the requirements of Eurocode 5.

The second set consists of 6 specimens that are also unprotected and outdoor exposed, without loading. Finally, the third set consists of 6 reference specimens stored indoors without loading in a room at constant RH and temperature. These specimens will provide a reference for the evolution of mechanical properties in stable storage conditions. The ageing campaign began in August 2021.

2.2 Instrumentation

To measure the evolution of the moisture content inside the beams as well as the shrinkage/swelling phenomena, the specimens are instrumented with three moisture content sensors and two strain gauges (Fig. 2a, b,c). 6 specimens per series are connected to the monitoring system. The moisture measurement is derived from a DC resistance measurement between two copper patches glued to the intermediate lamella of glulam specimens (Li et al. 2018). The resistance levels in wood for this configuration can reach 1 Giga Ohm for moisture contents around 10%. Considering the numbers of sensors, the resistance levels and the need of simultaneous strain and MC measurements, no commercially available solution was adequate. Therefore, the monitoring system was developed in our laboratory and calibrated for these samples with calibration curves made under controlled environment for different temperatures and relative humidities (Uwizeyimana et al. 2020). As the MC measurement is impacted by temperature (Forsén and Tarvainen 2000), compensation of temperature is carried out following the law presented by Uwizeyimana et al. (2022). Temperature measurement is made using thermocouples integrated into specific specimens exposed to the same conditions as monitored specimens to avoid possible interferences between the different sensors. Data are collected on each sample by dedicated measurement electronic cards and transmitted by radio to an acquisition centre located about ten metres away from the test area (Fig. 2d). On each set of 6 specimens, data is collected every 10 min, for a total of 36 moisture sensors and 24 strain gauges.

The strain gauges (K-CLY4x-10/350) are glued to the upper and intermediate lamellae on either side of the glue joint respectively (Fig. 2a). Given the thickness of the gauges in relation to the glue joint, they are not positioned on the same vertical axis to limit the risk of delamination. The gauges are therefore placed on either side of the specimens 60 mm from the ends.

Outside temperature and RH data are measured locally by a dedicated sensor and weather and rainfall monitoring is carried out by data collected by the weather station at nearby Tarbes-Ossun-Lourdes airport. The data are collected by the Infoclimat association (Infoclimat 2023).

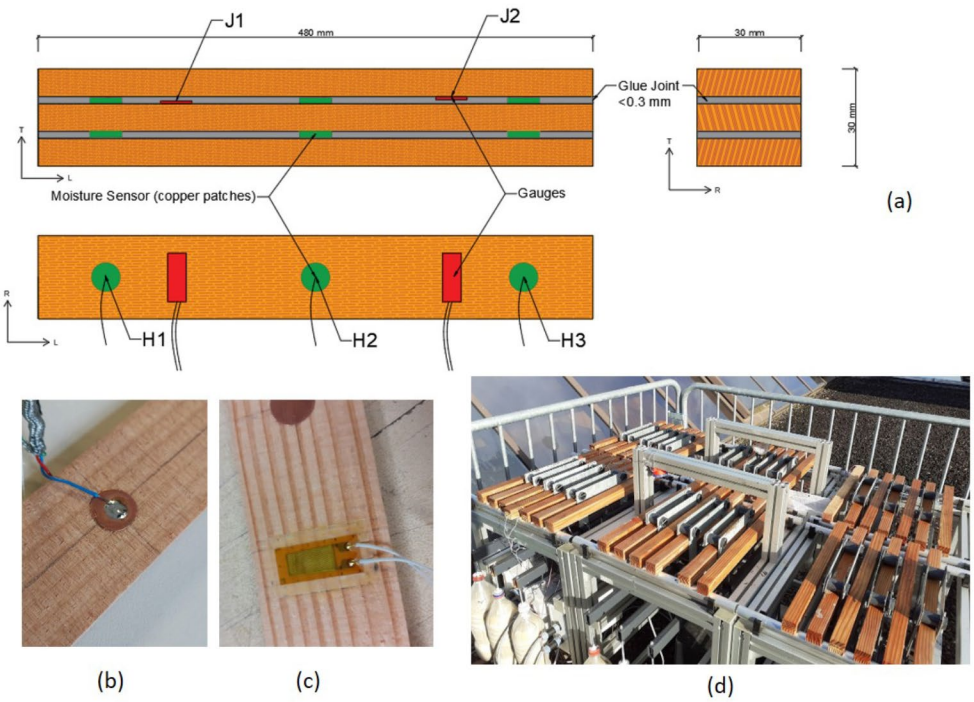

Fig. 2 Layout of an instrumented specimen, H1, 2 and 3 are moisture sensors, J 1 and 2 are strain gauges (**a**), Copper patch for moisture content measurement (**b**), strain gauges (**c**), outside exposed samples (**d**)

2.3 Mechanical characterization

The effect of W/D cycles on the mechanical properties of glulam is evaluated in shear and bending. Shear tests evaluate the evolution of the mechanical strength of glue joints, while 4-point bending tests evaluate the evolution of the mechanical strength of glulam under loads representative of the stresses encountered in bridges. The mechanical tests are carried out on samples stabilised for 15 days at 20 °C and 65%RH in a climatic chamber (WEISS C/340/40/3), leading to a MC in the wood of 12% ± 1% limiting the effects of variable MC on wood and adhesive bonds strength between our samples (Lu et al. 2024).

2.3.1 Shear tests

These tests are adapted from Annex D of the EN 14080 (2013) dedicated to the characterization of glulam joints. In order to have an analysis of the shear stress over the entire length of the sample, one specimen of each series was cut into 14 cubes of 30 mm on each side and the upper glue joint was shear tested. Only the upper joint could be tested, as the shear test on the upper joint damages the lower one, which, therefore, can't be properly evaluated. The delamination rate of each sample was measured in accordance with Annex D of EN 14080 (2013). The results of this small-scale samples could then be adapted to larger scales, considering the size effects on wood and glue joints mechanical performance (De Santis et al. 2023). All lamellae have similar wood orientation and glue joints were tested in the longitudinal direction of wood limiting the effect of wood fibre direction on the bonding performance between our samples (Kaya and Karagüler 2024). The assembly described in the standards was adapted to the size of our samples (Fig. 3).

To ensure alignment of the adhesive joint with the shear plane of the test fixture, a wedge is glued to the lamella adjacent to the joint. The shear stress is determined by the following equation:

$$\sigma_{vmax} = \frac{F_{max}}{bh} \tag{3}$$

Where:

- σ_{vmax} : The shear stress (MPa);
- F_{max} : The force applied to the sample (N);
- b, h : Respectively the base and height of the specimen (mm).

To complete the analysis of glue joints damage, flexural tests are carried out on the specimens.

2.3.2 4-point bending tests

The evolution of the instantaneous mechanical properties of the specimens is studied in 4-point bending in accordance with EN 408 (2012) (Fig. 4).

The tests are carried out using an MTS100 electromechanical testing machine with a 100 kN load cell. The strain measurement in the centre of the specimen is carried out via

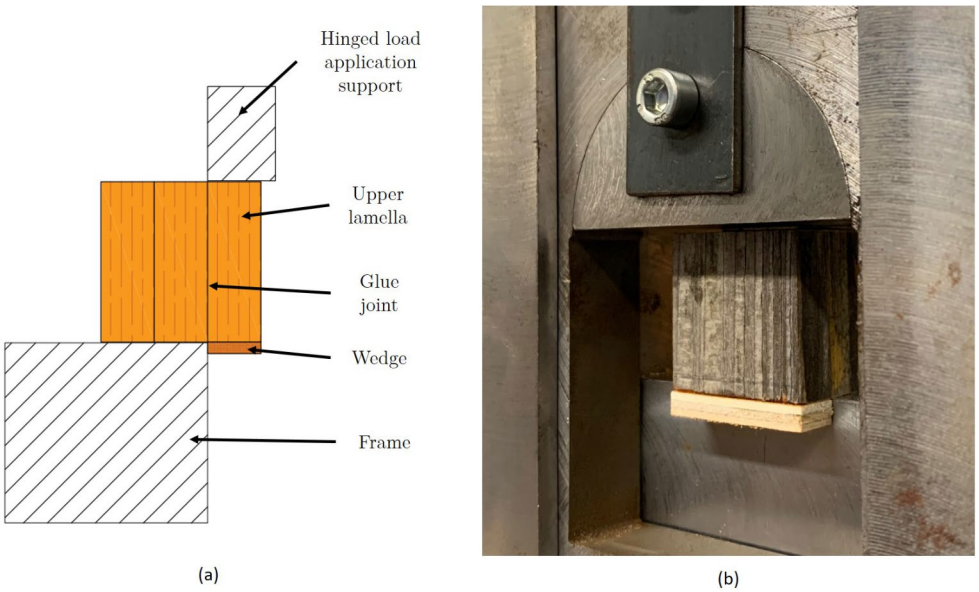

Fig. 3 Scheme of the shear test device (**a**), glulam sample being tested (**b**)

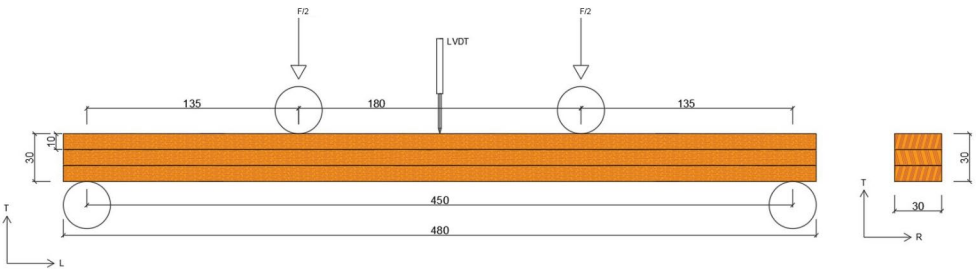

Fig. 4 Illustration of the 4-point bending tests

a Solartron AX5S LVDT. The mechanical tests are filmed by a standard camera to allow a visual analysis of the fracture mechanisms.

The bending stress (σ_{max}) and Young's modulus (E) are determined according to the EN 408 (2012) with the following formulas:

$$\sigma_{max} = \frac{3F_{max}\,a}{bh^2} \tag{4}$$

Where:

- F_{max}: The maximum force applied to the specimen (N);
- a: The distance between a lower support and the nearest upper support (mm);
- *b and h*: Respectively the base and height of the specimen (mm).

$$E = \frac{3al^2 - 4a^3}{2bh^3\left(2\frac{w_2-w_1}{F_2-F_1} - \frac{6a}{5Gbh}\right)} \tag{5}$$

Where:

- F_1, w_1 and F_2, w_2: The force (N) and strain (mm) at 10 and 40% of *Fmax;*
- a: The distance between a lower support and the nearest upper support (mm);
- *b*, *h and l*: Respectively the base, height and span of the specimen (mm);
- *G*: The shear modulus, according to standard EN 408 for Douglas = 650 MPa.

3 Results and discussions

3.1 Monitoring of durability indicators

Specimen tracking data and weather data are stored on a dedicated server. An interface and a processing system made on R (R Core Team 2022), displays MC, deformation and rainfall values as a function of time. The sampling period is 10 min. An hourly average is made to speed up the processing and display of the data. The program preprocesses the data by removing outliers using a Hampel filter (Hampel 1971). Smoothing can be achieved by a rolling average (Rehomme and Ladiray 1994) whose range can be

Fig. 5 Monitoring of durability parameters in exterior specimens (raw moisture data (average of 3 sensors) and strain (average of both gauges) of an outdoor specimen)

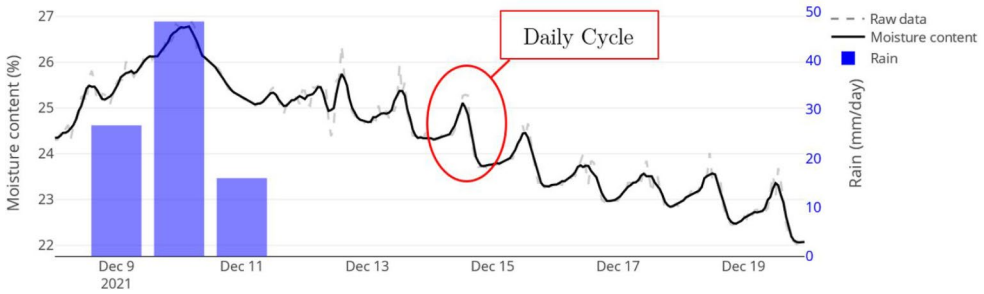

Fig. 6 Daily W/D cycles during a drying period (data from a representative outdoor specimen)

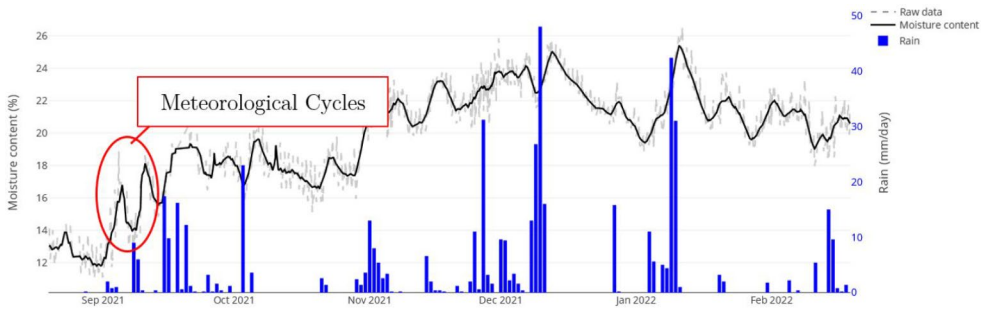

Fig. 7 Weather-related W/D cycles. The black curve corresponds to a smoothing over 48 h. The raw data is shaded (data from a representative outdoor specimen)

defined from 1 h to 30 days to observe short- and long-term phenomena. Different smoothing scales allow to highlight characteristic phenomena from different time scales.

The monitoring of durability indicators via sensors integrated into glulam showcased humidity variations and deformations on 12 external specimens (6 loaded and 6 non-loaded) from September 2021 to February 2022 (Fig. 5). The measurements carried out are homogeneous for all external specimens.

Several scales of humidification and drying cycles in wood can be observed and will be presented in paragraph § 2.1.1. These scales are: short-term, day/night variations; medium-term, weather-dependent cycles; and long-term, summer/winter seasonal cycles.

The correlation of moisture measurements with deformations observed in Fig. 5 highlights the effect of W/D cycles on deformations in glulam. The results obtained via the gauges positioned on either side of the adhesive joint allowed us to subsequently link these deformations with internal stresses at the adhesive joint (§ 2.1.3).

3.1.1 W/D cycles measured outdoors

The analysis of measurements over short periods of time (few days), shows the daily cycles (Fig. 6) which are related to the difference in humidity between day and night. These cycles are particularly noticeable during drying periods (e.g., December 13–19 in Fig. 6). While during periods of rainfall (e.g., December 9–11 in Fig. 6), these cycles are masked by the continuous increase in wood moisture content.

The daily W/D cycles over the first 6 months of measurement show a range of around 0.5 to 3% humidity between the high values obtained at the end of the morning and the low values obtained at the end of the day.

The second type of cycle measured is related to local rainfalls. The monitoring of rainfall data highlights “meteorological” W/D cycles, i.e. linked to local weather conditions in the short term. Moisture data have been smoothed using 48 h rolling average to hide daily cycles, the raw data are shaded. The firsts remarkable “meteorological” cycles are shown in red in Fig. 7.

These cycles of varying lengths are correlated to periods of humidification that can last from a few hours to several

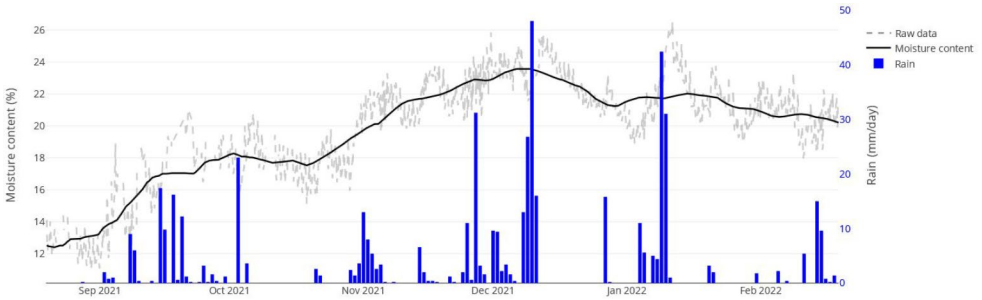

Fig. 8 W/D cycle related to the transition from summer to winter. The black curve corresponds to a smoothing over one month. The raw data are shaded (data from a representative outdoor specimen)

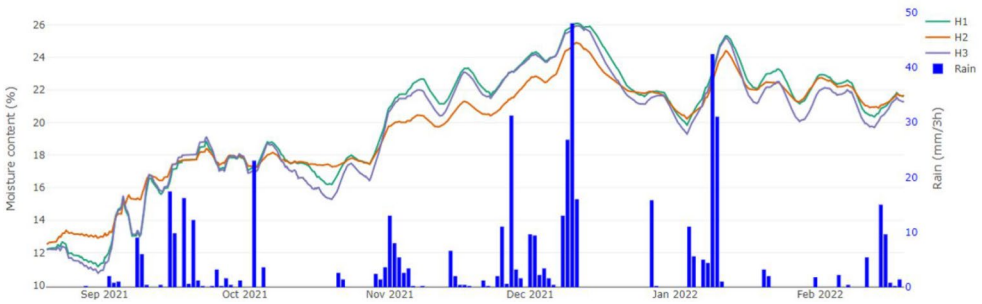

Fig. 9 Evolution of humidity as a function of the measuring area (data from a representative outdoor specimen)

days during rainfall episodes, followed by a more or less rapid drying phase depending on the weather conditions. The amplitude of moisture content in wood for these cycles varies from 1 to 5% over the considered period.

After 6 months of measurements, the effect of the transition from summer to autumn seems to lead to a third type of W/D cycle with a greater amplitude of about 10% (Fig. 8). Between September and February, MC increases until it peaks in mid-December. A drying phase then takes place until February and should continue during the spring and summer period. The MC data were smoothed by making a monthly rolling average to hide the daily and meteorological cycles.

The MC measured in these external specimens is consistent with the measured weather and the MC measured in sections of monitored bridges that varies between 10 and 25% (Norberg 1999; Tannert et al. 2011; Dietsch et al. 2014; Koch et al. 2016; Bjorngrim et al. 2016; Franke et al. 2016, 2019; Fortino et al. 2019). MC measurements were used to identify different types of wet-dry cycles. Each type of cycle has specific characteristics in terms of duration and amplitude. The study of the evolution of the long-term mechanical properties will make it possible to establish the link between these cycles and the damage of the material.

3.1.2 Effect of moisture diffusion in wood on measurement

The amplitude of the W/D cycles varies with the position of the measurement along the specimens. This difference is particularly noticeable at the level of seasonal cycles (Fig. 9). Indeed, during a period of rain, the MC in the centre of the specimen (H2) increases less than the MC on the edges (H1 and H3) with a difference of about 1.5% between the maximum MC at the extremities and at the centre of the specimens. Conversely, during the drying phases, the MC at the ends of the specimens becomes lower than that in the centre of the specimen with a difference of -2% when the minimum MC was reached in September 2021.

The variations in MC measured in wood imply shrinkage and swelling phenomena in the material which can lead to degradations of the wood lamellae (Angst-Nicollier 2012) and the glue joints due to the relative deformations of the different lamellae (Yelle and Stirgus 2016). However, the impact of these shrinkage and swelling phenomena on the mechanical bending properties of GLT in outdoor use still remains up until today unexplored and poorly documented. In this context, the monitoring of W/D cycles and their correlation with shrinkage/swelling phenomena would give a better understanding of degradation phenomena.

3.1.3 Shrinkage and swelling

Built-in strain gauges in the lamellae are used to measure shrinkage/swelling in the radial direction of specimen lamellae (Fig. 2). As the shrinkage-swelling phenomenon is mainly related to variations in the bound water content of the wood, the correlation between the average MC measured by the patches (H1-H2-H3) and the average deformation (J1-J2) (Fig. 5) confirms the relevance of the moisture measurement to identify the conditions leading to the generation of internal stresses that can damage the material. In our case, the deformations are measured between − 2,600 µm/m at 10% MC and 9,100 µm/m at 24.5%MC. This total deformation of 11,700 µm/m for a MC amplitude of 14.5% corresponds

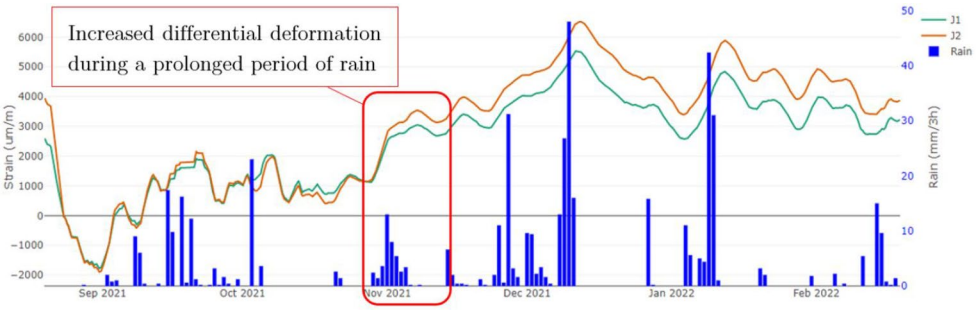

Fig. 10 Gauge deformations on either side of the glue joint, 48-hour rolling average (data from a representative outdoor specimen)

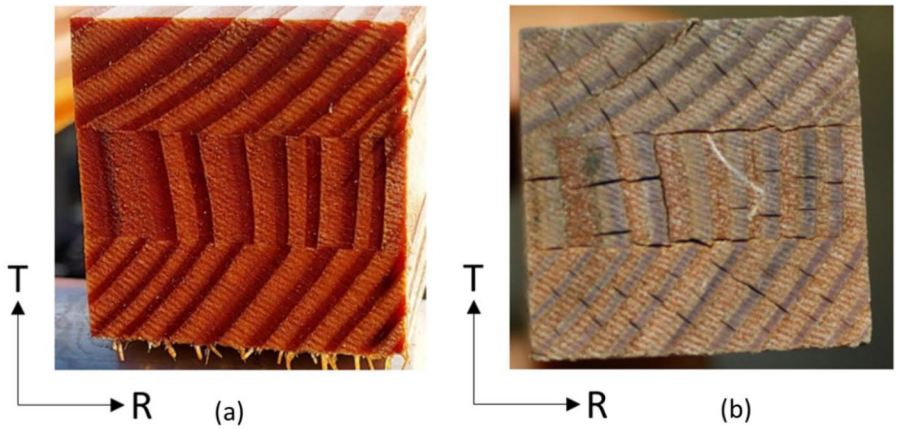

Fig. 11 End of a specimen before (**a**) and after (**b**) a period of 6 months outdoors

to a shrinkage coefficient (Cr) of 0.08. The shrinkage coefficient describes the rate of deformation per percent change in MC as follows:

$$C_r = \frac{\Delta_{def}\,(\%)}{\Delta_{MC}\,(\%)} \tag{6}$$

In climatic chambers, shrinkage coefficients of 0.11 were measured on Douglas GLT specimens (Uwizeyimana et al. 2023). In the literature, the common coefficient of shrinkability of Douglas fir in the radial direction is 0.14 (Glass and Zelinka 2010). The measured deformations are therefore relatively small compared to the data in the literature. However, since the measured humidification phases are related to exposure to rain, open water could be partly responsible for the measured humidity variations without causing deformations. Variations in humidity measured between the centre and the extremities of the specimens are around 2% (Fig. 9). With the shrinkage coefficient of 0.08, it would mean differential deformations of 1,600 µm/m. In the literature, moisture gradients from 1.8% can be the cause of cracking related to tension perpendicular to the wire for spruce (Franke et al. 2019) which has a tensile strength perpendicular to the fibers equivalent to Douglas fir.

By analysing the two sets of gauges (J1 and J2), it appears that since the start of the tests, the gauges glued to the upper lamella of the specimens (J2) have had greater amplitudes than the gauges glued to the intermediate lamella (J1) (Fig. 10). As the upper lamella is the most exposed to weathering and solar radiation, it undergoes greater deformations with an amplitude of 8,500 µm/m compared to 7,500 µm/m for the intermediate lamella. We also observe that the differences in deformation between the lamellae increases during the humidification phases, particularly after a prolonged period of rain (6% increase in humidity in 8 successive rainy days) in November 2021 (Fig. 10). These differential deformations have been identified in the literature as a factor that can generate damage in glue joints (Koch 1967; SETRA 2006; Yelle and Stirgus 2016; CECObois 2020).

To characterize the impact of these stresses on the mechanical strength of the samples, shear tests on the adhesive joints and bending tests were performed.

3.2 Mechanical characterization

3.2.1 Evolution of the shear properties of adhesive joints

W/D cycles generate shear stresses on the adhesive joint (Koch 1967; SETRA 2006; Yelle and Stirgus 2016; CECObois 2020) The repetition of these cycles damages the wood and the glue joint, leading to the creation of cracks and delamination phenomena. Observations were made on all specimens. Important cracks and delamination were noted at the ends of the specimens (Fig. 11) while the delamination on the lateral faces of the specimens, on the other hand, are very shallow.

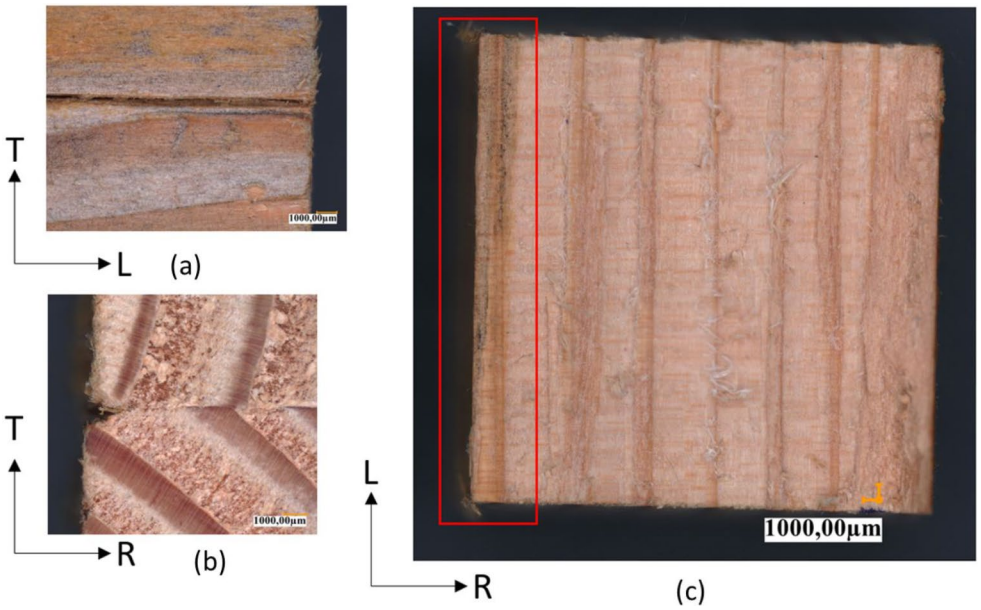

Fig. 12 Maximum delamination observed after 6 months of outdoor exposure, as seen from the outside (**a**) as seen from the flow rate before fracture (**b**) as seen from the post-fracture bonding interface (delaminated area outlined in red) (**c**)

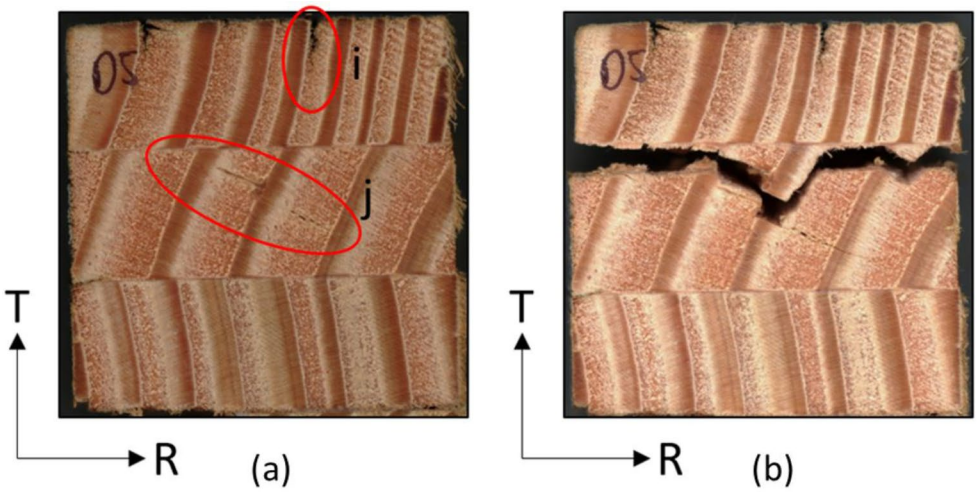

Fig. 13 Pre-fracture facies (**a**), fracture facies during shear tests (**b**)

The maximum measured depth on the side of outside exposed specimens was 2 mm on an unloaded outer specimen (Fig. 12) and three specimens with a delamination depth of 1 mm. There is no measurable delamination for the loaded outer specimen.

Cracks close to the interface between the early and late wood that can reach the glue joint were observed on the upper lamella of the specimens, which is most exposed to rain and sun (Fig. 13). Cracks in the radial direction are also observed, depending on their position, seem to have an impact on the shear failure. For example, the specimen has a crack in the wood near the glue joint (Fig. 13). In this case, the fracture during the shear test occurred in this defect and not in the adhesive joint (Fig. 13). This type of age-related cracking therefore locally creates shear brittleness.

Figure 14 shows the results of the shear tests on the 14 cubes cut from a specimen exposed for 6 months outdoors. The cubes cut at the ends behaved differently from the other 12 samples and were not included in the comparative results between the different ageing conditions. Indeed, due to their exposure, their damage is not homogeneous and representative of the general condition of the specimen. The ends of the specimens are indeed more exposed to climatic constraints because the face in the unprotected RT plane is very sensitive to humidity variations (Monteiro et al. 2020). We note cracks and delamination on these faces propagating up to 1 cm deep.

The results of the shear tests for the 12 samples cut in one specimen in each different ageing configuration were compared using Wilcoxon's nonparametric test (no normal distribution assumption) (Wilcoxon 1945). Tests carried out on specimen throughput show an average shear loss of about 21% for external specimens and 26% for loaded outer specimens (Fig. 15). The Wilcoxon test showed that

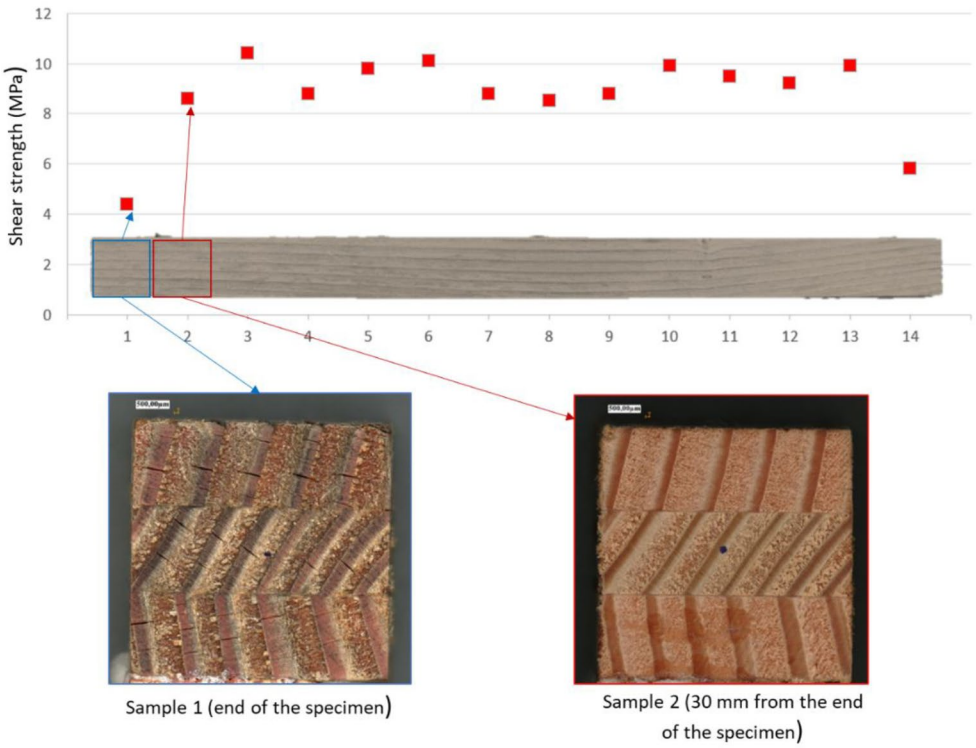

Fig. 14 Evolution of shear strength of the 14 samples (horizontal axis) cut from one specimen, sample 1 illustrates the damage occurring at the end of the specimens compared to the other samples cut within the beam such as sample 2

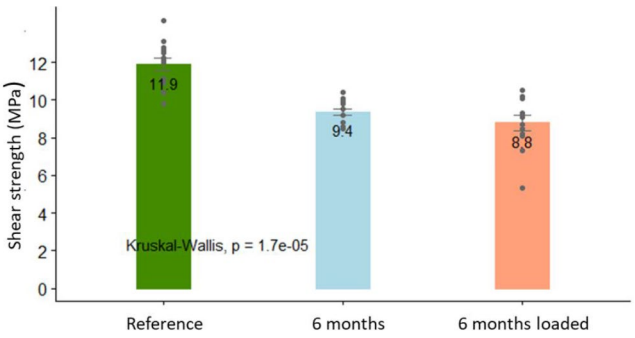

Fig. 15 Evolution of shear strength for different ageing conditions

loaded and unloaded samples for 6 months resulted in a statistically significant decrease in maximum shear strength ($p = 0.0000798$ and $p = 0.0000783$ respectively). There was no statistically significant difference between loaded and unloaded cases ($p = 0.418$). The results obtained for specimens that spent 6 months outdoors are consistent with the literature (Yanagawa and Masuda 2011). This remarkable decrease in shear strength confirms that outdoor exposure is an important parameter in the ageing of glulam wood.

The dispersion of the results on these shear tests of the series "6 months outside loaded" indicates that the damage to the adhesive joint is not homogeneous. We measure a shear strength 50% lower for a sample of the loaded outer specimen compared to the average strength of the reference series, while we do not observe any macroscopic damage on this specimen. The delamination rates measured on the samples are relatively low after 6 months of aging with a maximum measured delamination depth of 2 mm and maximum delamination rates of 7% of the bonding surface. The loss of property measured in shear is not correlated with the delamination rate of the glue joint.

The measurement of delamination rates is therefore not sufficient to characterize the degradation of the adhesive joints. The results of the shear tests show an effect of climatic stresses on the mechanical properties of the joints. In contrast, the loading applied to the specimens did not have a significant effect on the shear fracture strength (Fig. 15). After 6 months of ageing, we didn't observe any evolution of the rupture mode of glue-lines as the rupture is mostly cohesive rupture in wood except for bonding interfaces between final wood of both lamellae where cohesive rupture within the glue occurs.

The loss of shear strength therefore does not appear to be related to a change in the properties of the adhesive joints but to the appearance of structural weaknesses in the bonding interface (Raknes 1997).

On each set of shear tests, the specimen cut in the centre part of the glulam beam contains a copper patch embedded in the glue joint (Fig. 16). A specific analysis was performed to verify that the presence of the patch does not affect the shear strength measurements.

There is no significant difference in shear strength between joints with or without patches, however, it is difficult to conclude due to the small number of samples involved. The patches therefore do not appear to degrade the

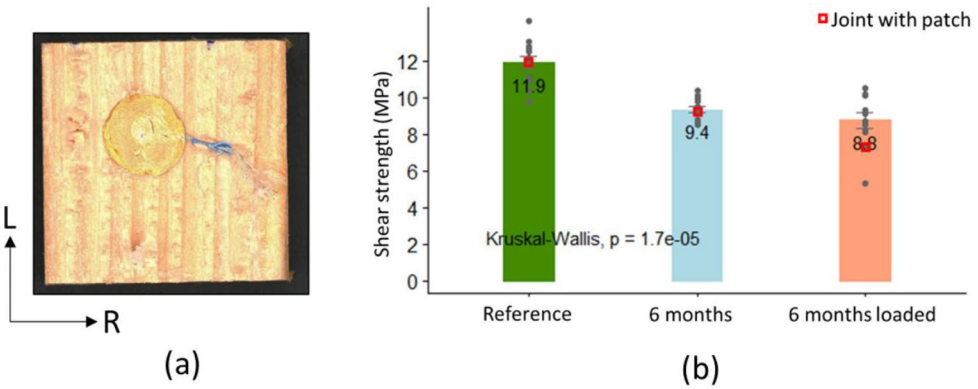

Fig. 16 Copper patches after shear tests (**a**), mechanical shear strength of joints with patch (**b**)

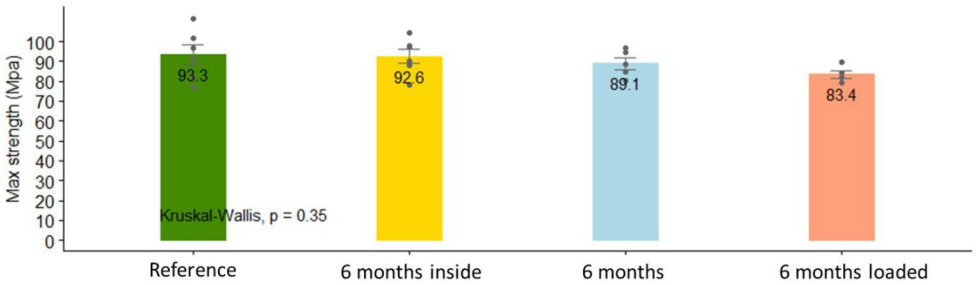

Fig. 17 Evolution of the stress at break as a function of ageing conditions

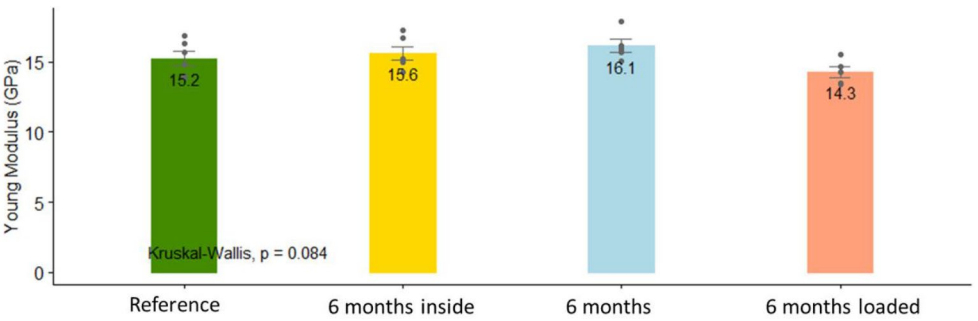

Fig. 18 Evolution of Young's modulus as a function of ageing conditions

shear strength of the glue joints. Longer-term tests, and on a larger number of specimens, would confirm the effect of the presence of patches on the shear strength of the adhesive joints. We note that in the case of these specimens, the break at the patch is always at the interface between the adhesive side of the patch and the wood as the adhesive of copper tape is weaker than the PUR used to glue the lamellae.

3.2.2 Evolution of 4-point bending properties

In order to determine the effect of damage to glue joints and W/D cycles under real conditions on the instantaneous 4-point bending strength of glulam, a test campaign was carried out after 6 months. 6 specimens from the "reference" and "6 months inside" sets, as well as 5 specimens from the "6 months out" and "6 months outer loaded" sets were tested in 4-point bending. The 6th specimen of these series was used for shear tests. A decreasing trend in bending strength is observed (Fig. 17) with an average loss of 5% for external specimens and 11% for loaded external specimens. However, given the standard deviation of our tests and the small number of samples, these differences are not significant at the 0.05% criterion.

There is also no remarkable evolution on the Young's modulus (Fig. 18). The results of the mechanical tests of the specimens aged outdoors for 6 months do not show significant losses of properties. Other studies highlight the absence of an effect of aging on Young's modulus after two years of outdoor exposure (Humar et al. 2020).

Even if a slight trend seems to be emerging in terms of fracture stresses, the losses of mechanical properties over these first 6 months of exposure do not show any significant changes. If we compare these first results with information from the literature and the results obtained under accelerated aging conditions, it would seem that the accelerated W/D cycles are very severe compared to the natural cycles measured during these first 6 months of exposure. Indeed, the decrease in flexural strength after a single accelerated W/D cycle in a climatic chamber is around 15% (Uwizeyimana et al. 2022) with 11-day cycles (5 days at 35 °C/98%RH,

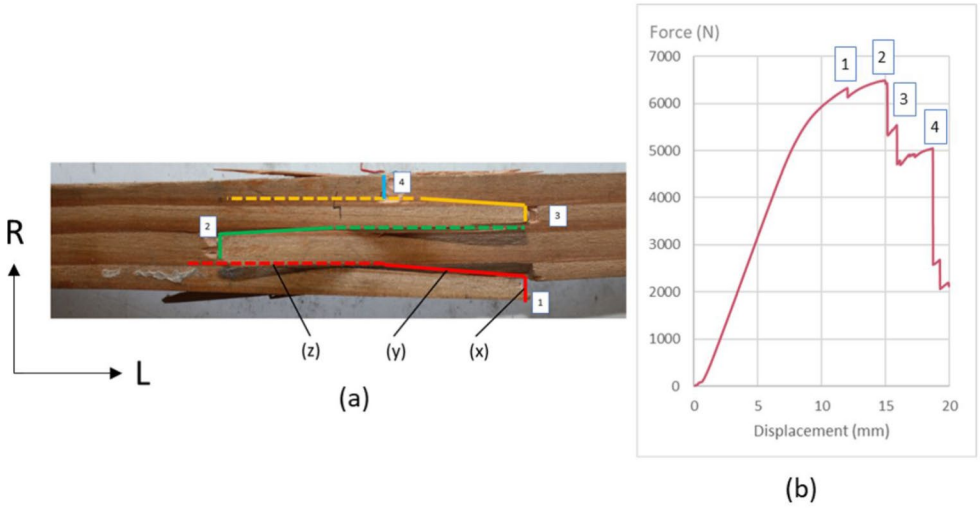

Fig. 19 Fracture mode A: crack in the RT plane in the spring wood (x), crack with an angle of the order of 3° to the TL plane in the summer wood (y), crack in the TL plane at the interface between the spring wood and the summer wood (z) (**a**); Force/Displacement curve associated to the fracture mode A (**b**)

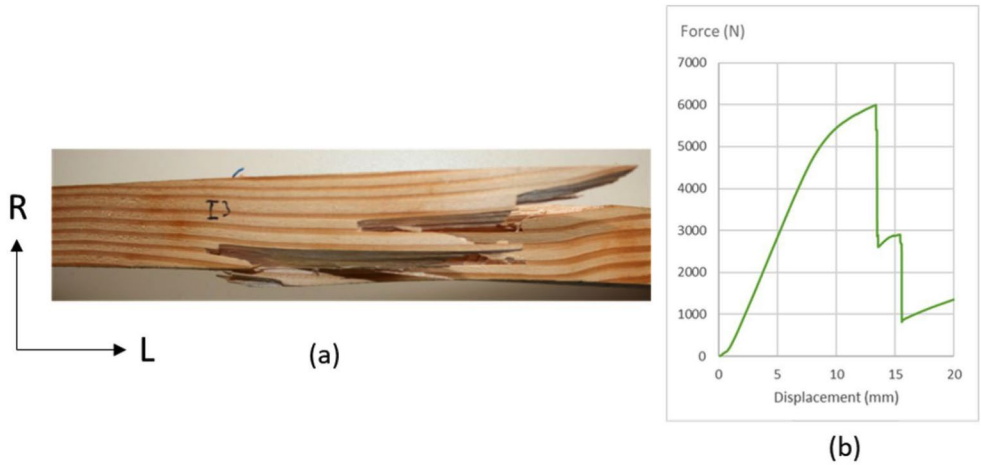

Fig. 20 Fracture mode B: underside view after failure (**a**), force/displacement curve associated to this rupture (**b**)

1 day immersed and 5 days at 35 °C/50%RH). The long-term monitoring of the outside cycles and the evaluation of the mechanical properties in bending will allow us to determine more precisely the impact of natural W/D cycles on the durability of the material and to correlate our results more precisely with those obtained on accelerated tests.

Beyond the evolution of mechanical properties, we observe a change in the behaviour during the failure of the specimens as a function of aging.

2.2.3

3.2.3 Evolution of rupture mechanisms

- In bending tests, we observe four main fracture modes.
- Fracture Mode A (Fig. 19): Sequential rupture where the growth rings break successively one by one or in small groups. The origin of this type of rupture is not identified in the literature;
- Fracture Mode B (Fig. 20): Abrupt failure of the tensile zone with a spike shape characteristic of a tensile fracture (Bodig and Jayne 1982);
- Fracture Mode C (Fig. 21): A sudden failure in which the tensile part breaks sharply perpendicular to the grain. This is a simultaneous rupture of all rings, characteristic of a brittle rupture of the tense area (Bodig and Jayne 1982);
- Fracture Mode D (Fig. 22): Longitudinal shear fracture (Pluvinage Guy 1992) in the glue joint.

The Mode A fracture mode has a characteristic force-strain curve with several load drops corresponding to successive ring failures (noted 1,2,3,4 Fig. 19). There is a succession of small ruptures before the failure of the specimen. Fracture is usually initiated on a ring at the edge of the specimen with crack propagation in the RT plane in spring wood. The crack then propagates at a shallow angle to the TL plane in the late wood. The crack spreads at the interface between the early and late wood for several centimetres. Either propagation in the longitudinal direction stops when the crack reaches the

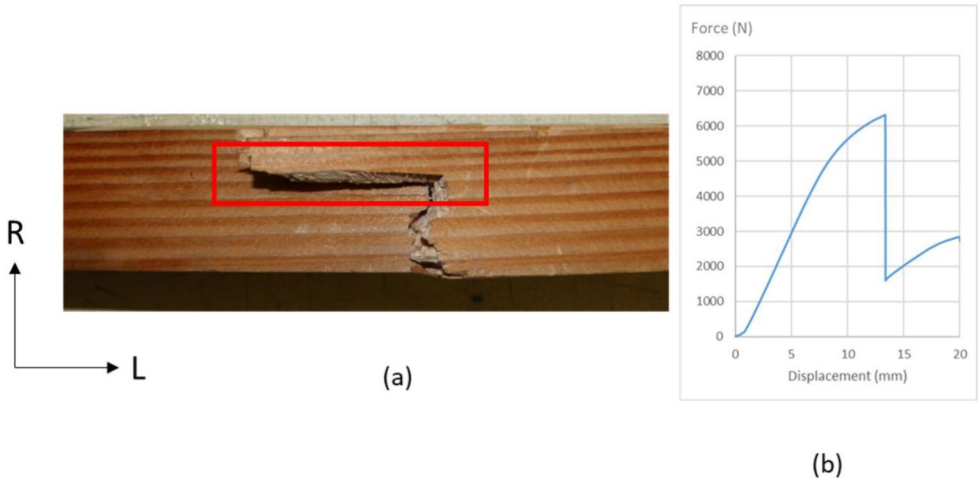

Fig. 21 Fracture mode C: underside view after failure (**a**), force/displacement curve associated to this rupture (**b**)

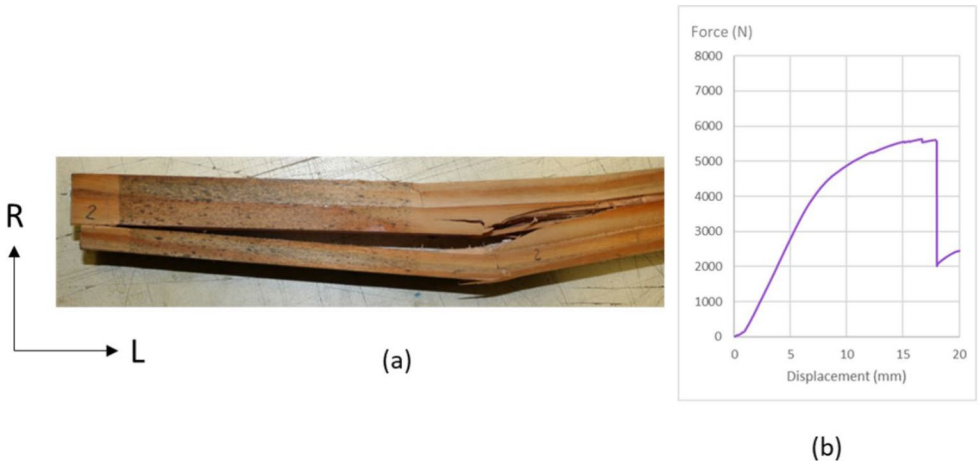

Fig. 22 Fracture mode D: lateral view of a specimen after failure (**a**), force/displacement curve associated to this rupture (**b**)

area between the lower and upper supports of the loading system, or it initiates a new fracture in the adjacent ring. The rupture of each ring is abrupt (noted 1,2,3,4 in the order of appearance in Fig. 19).

The Mode B fracture mechanism (Fig. 20) is characterized by a sudden failure of the specimen with a bursting of its lower part. All rings break at the same time.

The tensile fracture surface is highly variable depending on the specimen. Depending on the case, the rupture occurs between groups of rings, causing a rather clear break over the width of the specimen, or individual fibers tend to separate, resulting in a break with very pronounced spikes. After burst failure, the cracks open until the end of the test and the failure of the specimen.

The Mode C fracture (Fig. 21) is characterized by a sudden failure of the specimen with a clear fracture in the RT plane.

In some cases, the crack propagates a few centimetres in the TL plane (red box in Fig. 21) at an interface between the late and early wood before continuing to propagate perpendicular to the grain.

The Mode D fracture mechanism (Fig. 22) describes a shear failure of the glue joint in the LR plane. This mechanism is characterized by a long loading bed before breaking compared to other types.

The shear fracture resulted in a complete failure of the glue joint over the entire sheared area between the lower and upper supports of the loading device. The fracture then spreads through the wood for a few centimetres between the inside supports. Sliding between the lamellae continues until the end of the test and the full failure of the specimen.

Flexural tests show that the ageing of specimens has an impact on the fracture mechanisms occurring in 4-point bending (Fig. 23).

Of the 22 specimens tested in bending to date, mode A (sequential fracture mode) is mainly encountered on specimens that have not undergone W/D cycles (Fig. 24). Only 4 out of 12 specimens that have not undergone the W/D cycles have abrupt failures of Modes B or C. Mode C occurs in the majority of outdoor exposed specimens (Fig. 24). The evolution of these fracture modes therefore indicates an evolution towards abrupt ruptures after aging.

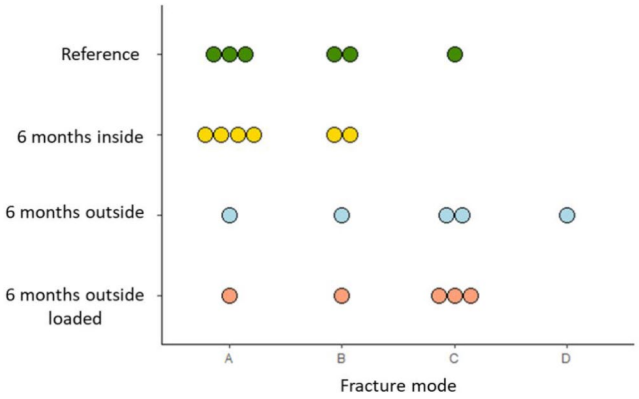

Fig. 23 Evolution of failure modes as a function of ageing conditions

These results are consistent with trends observed during accelerated W/D cycles on similar specimens (Uwizeyimana et al. 2022) and on solid wood (Kránitz et al. 2016). Regarding the fracture mode D, the decrease in the shear strength of the adhesive joint, with bonding zones with very low strength values, may explain its appearance. If the weakest bonding areas are in the shear stressed zone during the bending tests, they could initiate the shear fracture in the adhesive joint during the bending tests.

4 Conclusion

Three series of specimens were studied during a 6 months ageing period with a monitoring of durability indicators. The analysis of these results highlights the following conclusions:

- The monitoring set up has clearly shown its potential to record the evolution of MC and deformations locally, within the lamellae of glulam samples.
- The recorded MC variations clearly show different scales of W/D cycles. Daily cycles show variations in humidity of between 0.5 and 3% while weather cycles show variations between a rainy and dry period of up to 5%. Regarding the seasonal cycles, a maximum MC amplitude between summer and autumn of 10% could be observed. The correlation of the measurements with the local climatic conditions shows the reliability of this monitoring solution. Regarding the deformations, they are directly correlated with variations in MC.
- Deformations about 12 000 µm/m were measured for a moisture gradient in wood of 14.5%. The measured deformations are lower than those expected for such variations in humidity and could be explained by the presence of both free water and bound water in the wood during rainy periods. The comparison between the upper and intermediate lamellae shows a non-negligible differential strain of 1600 µm/m which may cause macroscopic cracks and delamination.
- Shear tests carried out after 6 months of outdoor exposure indicate that degradation has already occurred between August 2021 and February 2022 at the adhesive joints with a significant decrease of more than 20% in their strength. The instrumentation of the specimens with patch sensors had no effect on the resistance of the adhesive joint. Macroscopic observations of specimens and measurement of delamination rates donot highlight any relation between the visual condition of the specimens and the shear properties.
- The 4-point flexural tests do not show significant losses in the properties of the specimens at this stage of ageing,

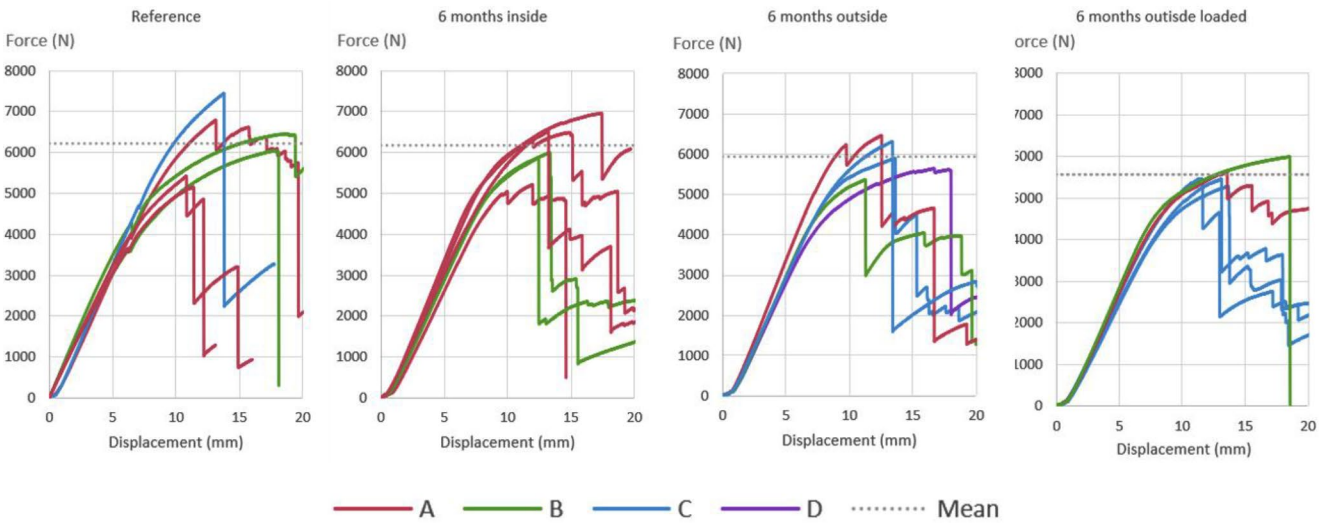

Fig. 24 Force-displacement curves during 4-point bending tests

i.e. after 6 months outdoors, whether for loaded or unloaded specimens. The results of bending tests after longer exposure times will be used in the future to support these initial results.

- The failure mechanisms, on the other hand, evolve with the aging of the specimens. Indeed, more abrupt fractures for externally aged specimens have been observed. In addition, the decrease in the strength of the glue joints could be the cause of the shear fractures that appear on outside aged specimens during bending tests.

These first results demonstrate the interest of an integrated monitoring system to monitor the damage of glulam to evaluate the effects of W/D cycles. Glue joints are a specificity of this material that remains to this day the source of potential defects on engineering structures over time. The evaluation of their long-term performance and the development of embedded sensors that could evaluate the mechanical stresses within glue joints is essential to ensure an appropriate monitoring of infrastructures. In this context, these ageing tests will be continued over a period of 5 years by carrying out instantaneous fracture tests every 6 months. The ultimate objective will be to propose a damage model based on MC and deformations allowing site managers to plan the curative and preventive maintenance of their structures in an optimized manner.

Acknowledgements The research that led to the results presented received funds from the Region Occitanie, the Communauté d'agglomération Tarbes-Lourdes-Pyrénées and the Institut Universitaire de Technologie de Tarbes. The authors thank Emmanuel Laügt (IUT de Tarbes) for his contribution to the development of the monitoring system.

Author contributions G.G is the first author and the corresponding author, responsible for sample preparation and testing, data analysis, and the preparation of the paper. L.E provided technical support for the development of the monitoring system and the data analysis and comments for the paper. M.P provided technical guidance for the research, the preparation of the paper and comments for the paper. F.E provided technical support for samples preparation and in bending testing, technical guidance for the research and the preparation of the paper and comments for the paper.

Funding Open access funding provided by Université Toulouse III - Paul Sabatier.

Data availability No datasets were generated or analysed during the current study.

Declarations

Competing interests The authors declare no competing interests.

References

Angst-Nicollier V (2012) Moisture induced stresses in glulam. Ph.D. Norwegian University of Science and Technology, p 138

Armstrong LD, Christensen GN (1961) Influence of moisture changes on deformation of Wood under stress. Nature 191:869–870. https://doi.org/10.1038/191869a0

Bjorngrim N, Hagman O, Wang X (2016) Moisture content monitoring of a timber Footbridge. BioResources 11:3904–3913

Bodig J, Jayne BA (1982) Mechanics of wood and wood composites. Van Nostrand Reinhold, New York

CECObois (2020) Guide sur la durabilité des ponts en bois (Guide to the durability of wooden bridges)

De Santis et al (2023) Evaluation of the shear size effect in glued laminated timber using a stochastic FE model calibrated on 17000 glue-line tests. Constr Build Mater 399:132488

Dietsch P, Gamper A, Merk M, Winter S (2014) Monitoring building climate and timber moisture gradient in large-span timber structures. J Civil Struct Health Monit 5:153–165

Ehrhart T, Grönquist P, Schilling S et al (2021) Mechanical properties of European beech glulam after 32 years in a service class 2 environment. https://doi.org/10.3929/ETHZ-B-000506091

EN 1995-1-1 (2005) Eurocode 5 - design of timber structures – part 1–1. General - common rules and rules for buildings

EN 1995-2 (2005) Eurocode 5 - design of timber structures– part 2. Bridges

EN 335 (2013) Durability of wood and wood-based products — use classes: definitions, application to solid wood and wood based products

EN 408 + A1 (2012) Timber structures - structural timber and glued laminated timber. Determination of some physical and mechanical properties

EN 14080 (2013) Timber structures - Glued laminated timber and glued solid timber - requirements

Forsén H, Tarvainen V (2000) Accuracy and functionality of hand held wood moisture content meters. VTT Publications 420, Otamedia Oy, Espoo, Finland

Fortino S, Hradil P, Metelli G (2019) Moisture-induced stresses in large glulam beams. Case study: Vihantasalmi Bridge. Wood Mater Sci Eng 14:1–15. https://doi.org/10.1080/17480272.2019.1638828

Fortino S, Hradil P, Koski K et al (2020) Health monitoring of stress-laminated timber bridges assisted by a hygro-thermal model for wood material. Appl Sci 11:98. https://doi.org/10.3390/app11010098

Fragiacomo M, Fortino S, Tononi D et al (2011) Moisture-induced stresses perpendicular to grain in cross-sections of timber members exposed to different climates. Eng Struct 33:3071–3078. https://doi.org/10.1016/j.engstruct.2011.06.018

Franke B, Franke S, Mueller A et al (2013) Long term monitoring of timber bridges - Assessment and results. Adv Mater Res 778:749–756

Franke B, Franke S, Müller A, Schiere M (2016) Long-term behaviour of moisture content in timber constructions – relation to service classes. Int Netw Timber Eng Res Meet Forty-Nine 5:19–23

Franke B, Franke S, Schiere M, Müller A (2019) Moisture content and moisture-induced stresses of large glulam members: laboratory tests, in-situ measurements and modelling. Wood Mater Sci Eng 14:243–252. https://doi.org/10.1080/17480272.2018.1551930

Glass SV, Zelinka SL (2010) Moisture relations and physical properties of wood. Wood handbook: wood as an engineering material: Chap. 4 Centennial ed General technical report FPL; GTR-190 Madison, WI: US Dept of Agriculture, Forest Service, Forest Products Laboratory, 2010: p 41–419 190:4.1-4

Grossman PUA (1976) Requirements for a model that exhibits mechano-sorptive behaviour. Wood Sci Technol 10:163–168. https://doi.org/10.1007/BF00355737

Gustafsson A, Pousette A, Björngrim N (2010) Health monitoring of timber bridges. In: Proceedings of 1st International Conference on Timber Bridges. Lillehammer, Norway

Hampel FR (1971) A general qualitative definition of robustness. Ann Math Stat 42:1887–1896. https://doi.org/10.1214/aoms/1177693054

Hearmon R, Paton J (1964) Moisture content changes and creep of wood. For Prod J 14:357–359

Hill CAS (2019) The environmental consequences concerning the use of timber in the built environment. Front Built Environ 5

Infoclimat (2023) Infoclimat -la météo en temps réel: observations météo en direct, prévisions, archives climatologiques, photos et vidéos… Accessed 5 Apr 2023 https://www.infoclimat.fr/

Humar M, Straže A, Šernek M et al (2020) Durability and mechanical performance of differently treated glulam beams during two years of Outdoor exposure. Drv ind (Online) 71:243–252. https://doi.org/10.5552/drvind.2020.1957

Hurmekoski E (2017) How can wood construction reduce environmental degradation? European Forest Institute 12

Kánnár A, Karácsonyi Zs, Andor K, Csóka L (2019) Analysis of glued-laminated timber structure during five years of outdoor operation. Constr Build Mater 205:31–38. https://doi.org/10.1016/j.conbuildmat.2019.01.234

Kaya TG, Karagüler ME (2024) The effects of wood fiber directions on bonding performance. Constr Build Mater 411:134625

Koch P (1967) Minimizing and predicting delamination of southern plywood in exterior exposure. For Prod J 17(2):41–47

Koch J, Simon A, Arndt RW (2016) Monitoring of moisture content of protected timber bridges. In: Proceedings of WCTE 2016 (World Conference on Timber Engineering). Vienna, Austria

Kránitz K, Sonderegger W, Bues C-T, Niemz P (2016) Effects of aging on wood: a literature review. Wood Sci Technol 50:7–22. https://doi.org/10.1007/s00226-015-0766-0

Kutnik M, Lepetit S, Nevé S (2011) Performance of Douglas-fir in real outdoor use conditions. In: 42th International Conference of the IRG Wood Protection

Legg C, Tingley D (2020) Timber bridge best practices and the state of the industry in Atlantic Canada. Wood Research & Development

Li H, Perrin M, Eyma F Moisture Content Monitoring in Glulam by Electrical Methods. In: Proceedings of 3rd International Conference on Timber Bridges. 27–29, Juin et al (2017) Skellefteå, Sweden, pp 80–89

Li H, Perrin M, Eyma F et al (2018) Moisture content monitoring in glulam structures by embedded sensors via electrical methods. Wood Sci Technol 52:733-752. https://doi.org/10.1007/s00226-018-0989-y

Lu P et al (2024) Influence of the moisture content on the fracture energy and tensile strength of hardwood spotted gum sawn timber and adhesive bonds (gluelines). Eur J Wood Prod 82(1):53–68.

Mårtensson A (1994) Mechano-sorptive effects in wooden material. Wood Sci Technol 28:437–449. https://doi.org/10.1007/BF00225463

Monteiro TC, Lima JT, Silva JRM da, et al (2020) Water flow in different directions in Corymbia citriodora wood. Maderas Ciencia Y tecnología 22:385–394. https://doi.org/10.4067/S0718-221X2020005000312

Norberg P (1999) Electrical measurement of moisture content in porous building materials. In: Eighth International Conference on Durability of Building Materials and Components (8DBMC), 30 May – 3 June. Vancouver, Canada, pp 1030–1039

Pittet V (1996) Etude expérimentale des couplages mécanosorptifs dans le bois soumis à variations hygrométriques contrôlées sous chargements de longue durée. https://doi.org/10.5075/epfl-thesis-1526. (Experimental study of mechanosorptive effect in wood subjected to moisture variations under controlled loads of long duration) (In French) Ph.D. dissertation, 1526, Ecole Polytechnique Fédérale de Lausanne (EPFL), Switzerland

Pluvinage Guy (1992) La rupture Du Bois et de ses composites (Wood and wood composites rupture) (in French). Cépaduès-Editions, Toulouse

Racher P, Biger J-P, Rouger F et al (1996) Structures en bois aux états limites: introduction à l'Eurocode 5: *Step 1 Matériaux et* bases de Calcul (Limit states design of wood structures: introduction to Eurocode 5) (In French). UNFCMP

Raknes E (1997) Durability of structural wood adhesives after 30 years ageing. Holz Roh- Werkst 55:83–90. https://doi.org/10.1007/BF02990523

Rehomme MG, Ladiray D (1994) Moyennes mobiles centrées et non-centrées. Construction et comparaison. (Centered and non-centered moving averages. Construction and comparison) (In French) Revue de statistique appliquée tome 42: 33–61

SETRA (2006) Les ponts en bois: Comment assurer leur durabilité. (Timber bridges: how to ensure their durability) (In French) Guide technique du SETRA (Service d'études technique des routes et autoroutes), France, ISBN: 9782110946553

Tannert T, Berger R, Vogel M, Liebhold P (2011) Remote moisture monitoring of timber bridges: a case study. In: Proceedings of the 5th international conference on structural health monitoring of intelligent infrastructure (SHMII-5), 11–15 December. pp 11–15

Uwizeyimana P (2021) Suivi de la santé structurale des infrastructures en bois par intégration de capteurs. (monitoring the structural health of wood infrastructures by integrating sensors). (in French) Ph.D. Université de Toulouse, Université Toulouse III - Paul Sabatier

Uwizeyimana P, Perrin M, Eyma F (2020) Moisture monitoring in glulam timber structures with embedded resistive sensors: study of influence parameters. Wood Sci Technol 54:1463–1478. https://doi.org/10.1007/s00226-020-01228-8

Uwizeyimana P, Perrin M, Laügt E, Eyma F (2022) Durability study of glulam timber under cyclic moisture loading. Constr Build Mater 315:125715. https://doi.org/10.1016/j.conbuildmat.2021.125715

Uwizeyimana P, Perrin M, Laügt E et al (2023) Strain measurement in glulam timber for bridges with embedded strain gauges and detection of moisture-variation effects. Wood Mater Sci Eng 0:1–11. https://doi.org/10.1080/17480272.2023.2165147

Wilcoxon F (1945) Individual comparisons by ranking methods. Biometrics Bull 1:80–83. https://doi.org/10.2307/3001968

Wood LW (1947) Behavior of wood under continued loading. US Department of Agriculture, Forest Service

Yanagawa Y, Masuda K (2011) Evaluation of bonding durability for wood preservative treated glulam by accelerated aging test and outdoor exposure test II bonding durability evaluated by outdoor exposure test and correlation to accelerated aging test. Mokuzai Gakkaishi 57:265–275

Yelle DJ, Stirgus AM (2016) Influence of anatomical, physical, and mechanical properties of diffuse-porous hardwoods on moisture durability of bonded assemblies. U.S. Department of Agriculture, Forest Service, Forest Products Laboratory, Madison, WI